Computers and Geotechnics 107 (2019) 55–67

Contents lists available at ScienceDirect

Computers and Geotechnics

journal homepage: www.elsevier.com/locate/compgeo

Research Paper

An experimental investigation of the microslip displacement of geological materials

C.S. Sandeep[a], K. Senetakis[b,*]

[a] Department of Architecture and Civil Engineering, City University of Hong Kong, Kowloon, Hong Kong Special Administrative Region
[b] Department of Architecture and Civil Engineering, Yeung Kin Man Academic Building, Blue Zone 6/F, City University of Hong Kong, Kowloon, Hong Kong Special Administrative Region

ARTICLE INFO

Keywords:
Tangential stiffness
Inter-particle friction angle
Micromechanics
Hardness
Roughness

ABSTRACT

We investigate the inter-particle tangential force–displacement behavior of a broad range of granular materials. The major experiments are conducted using a custom-built micromechanical loading apparatus and the emphasis of the work is placed on the microslip displacement. We show that for all the materials tested, the microslip displacement increases with the increase in normal force and that extended threshold displacements are observed for rougher and softer grains. An analytical expression proposed in the literature is modified, incorporating material micro-hardness in a normalized form, to establish an expression which can be used in micromechanical-based analysis of problems involving geological materials.

1. Introduction

Micromechanical-based analyses have helped researchers to improve their understanding on the complex behavior of granular materials including soils and fractured rocks as well as the analysis of large-scale and multi-scale problems [67,64,23–25,45]. The discrete element method (DEM) (after [14]) is one of the popular micromechanical-based computational tools in geomechanics research [50], which numerical tool has gained significant popularity in recent decades. Based on DEM or coupled FEM/DEM, studies into problems including penetration mechanisms [34], the behavior of railway ballast [43], and the mechanics of sand-silt mixtures [73] have been conducted providing important new insights into the complex behavior of granular materials. Through DEM, complex mechanisms of granular flows and landslides [65,44,38,63], the behavior of rocks and sandstone reservoirs [8,17], weathering and erosion processes [69] as well as the evolution of the micro-structure in particulate media [41] have been studied within a particulate framework. DEM has also helped researchers to explore geo-energy problems, for example the behavior of methane-hydrate bearing soils [36,35].

Important input parameters in DEM studies comprise the inter-particle coefficient of friction as well as the normal and tangential force – displacement relationships at the contacts of soil grains. Even though significant progress has been made in the development of contact models for unbonded and bonded grains (e.g. [37,31], DEM researchers need to make assumptions sometimes for the input properties to be used in the numerical analysis, which is majorly because of the limited available experimental data investigating the grain contact behavior of real soils [1,9]. Iverson et al. [33] mentioned that it is possible to obtain significant differences in the resultant output from different numerical models due to the lack of robust equations or parameter values. Cheung et al. [8], in their numerical study on the behavior of sandstone reservoirs, emphasized the importance in obtaining grain contact parameters in the laboratory which can enhance the state-of-the-art in the micromechanical-based study of complex granular materials. It is therefore stressed that further insights into the grain contact behavior of real soils are necessary to be obtained in the laboratory so that to enhance the state-of-the-art in geomechanics and provide a platform for more realistic models to be produced to be used as input in DEM studies.

DEM analyses commonly adopt the Hertz [29] and Mindlin and Deresiewicz [46] models to simulate the force – displacement relationship in the normal and tangential directions of the contacted grains, respectively (after [40,50]). Based on experiments on real soil grains and reference materials (e.g. chrome steel balls and glass beads), researchers have shown that the Hertz model can be used satisfactorily to fit the experimental normal force – displacement data obtaining useful information on the Young's modulus of the contacted surfaces. However, it has been reported that this model has a limitation on that it cannot capture the initial regime of soft behavior which is obtained for

* Corresponding author.
E-mail addresses: sschitta2-c@my.cityu.edu.hk (C.S. Sandeep), ksenetak@cityu.edu.hk (K. Senetakis).

https://doi.org/10.1016/j.compgeo.2018.11.013
Received 13 June 2018; Received in revised form 10 November 2018; Accepted 17 November 2018

Nomenclature

A_S	surface area of indenter
E	contact Young's modulus
E^*	equivalent Young's modulus
ΔE	percentage energy loss
F_N	normal force
F_{Tx}	tangential force at shearing displacement x
G	shear modulus of the material
h	indentation depth
H	Martens hardness
H_N	normalized hardness
K_T^0	intial tangential stiffness from M-D
K_T^x	tangential contact stiffness at any displacement x
K_T^{2exp} and K_T^{2the}	experimental and theoretical tangential contact stiffness at 0.0002 mm of tangential displacement
L	elastic energy stored
ΔL	area of closed loop
R	particle radius
u and v	number of points in the horizontal plane (for roughness measurement)
W	deviation of each point from mean height (for roughness measurement)
S_q	RMS roughness
α	contact radius
β	angle between faces of Vickers diamond pyramid
δ_N	displacement in the normal direction
$\delta_{T(\exp)}^{slip}$ and $\delta_{T(\text{the})}^{slip}$	experimental and theoretical (M-D) slip displacement
ν	material Poisson's ratio
μ	inter-particle friction

most materials [5,10,47,57,2]. In the tangential direction, there exist different elastic-plastic models (e.g. [70,3,74]), which focus, majorly, on the stick condition and they are derived, typically, on the basis of a limited spectrum of material types. In the recent work by Olsson and Larsson [51] for elastic-plastic materials, the slip behavior was accounted by considering different plastic responses and varying hardness. Many of the previous studies or developed models are typically limited to engineered materials, which might be due to the lack of sophisticated experimental data for real geological materials. This is particularly true for real soil grain contacts which follow the sphere-sphere (or grain-grain) configuration [6,61]. The studies by Nardelli et al. [48] and Sandeep et al. [54] reported that for real geological materials, the Mindlin and Deresiewicz [46] model showed poor fitting to the experimental tangential force – displacement data on Eglin sand and completely decomposed volcanic granules, respectively. It has been highlighted in these previous works that adjustments of theoretical models are needed to be considered so that better fitting can be applied to the force – displacement relationship of soil grain contacts.

In this study, the inter-particle tangential force – displacement relationship of different geological and reference grains was examined experimentally, with a focus on the slip (or microslip) displacement occurred from the laboratory tests. The determination of the slip displacement of contacted surfaces plays an important role in modeling as well as in characterizing the energy dissipation, fretting and damping [16,66,7,52,53]. This slip behavior is correlated with different properties of the tested materials including their friction, surface morphological and elastic characteristics as well as material hardness.

2. Materials

The micromechanical behavior of chrome steel balls (CSB) and three naturally occurred geological materials, which included Leighton Buzzard sand grains (LBS), crushed limestone (LS) and completely decomposed granite (CDG) were investigated in the current study. These materials were examined by Sandeep and Senetakis [56] with a focus on the inter-particle coefficient of friction at a steady-state sliding and its relationship with the surface roughness and the Young's modulus of the contacted surfaces. In the present study, the focus is the investigation of the force – displacement relationship of the different materials experimentally with emphasis on the role of material type on the occurred slip displacement.

In Table 1, the properties of the materials tested in the present study are summarized providing their basic characteristics. The LBS grains consist of quartz and they are fairly rounded and spherical in shape with relatively low roughness. The LS grains are composed of crushed non-clastic rock and they are irregular in shape. CDG is a weathered rock from Hong Kong, which material is of major interest in tropical and sub-tropical regions in geotechnical and infrastructure engineering as well as the study of landslides. It consists of irregularly shaped grains with very high roughness and part of the original minerals (majorly feldspars and mica) has been chemically altered to a clay coating on the surface of the grains. The three geological materials were mechanically sieved and grains from the fraction 1.18–3.00 mm from each material were used in the study. CSB are of 2 mm in diameter and they are included in this study, along with the three aforementioned geological materials, to investigate the differences in the slip displacement behavior across variable material types through micromechanical loading tests at the interfaces of grains.

The literature suggests that the behavior of interfaces of engineered and geological materials is significantly affected by surface roughness [20,28,26,27,56,55]. In the study, the roughness of the materials was measured with the Veeco NT9300 optical surface profiler at the City University of Hong Kong to incorporate, qualitatively, this parameter in the analysis of the micromechanical test results. The vertical scanning interferometry (VSI) mode was chosen to obtain the surface roughness owing to its capability to scan large areas of heterogeneous materials [13]. This VSI mode in the current optical surface profiler allows non-destructive evaluation of the surface roughness with a high resolution of 0.1 nm. As described by Sandeep and Senetakis [56], for the measurement of roughness for the different grains, a field of view of 20x20μm was chosen, similar to previous studies by [60,62], and the effect of the curvature was removed. The surface roughness is presented as the root mean square (RMS) roughness denoted as S_q based on Eq. (1).

Table 1
Properties of the materials tested in the study.

Material code	Material description	Diameter (mm)	Surface roughness (S_q) (nm)	Hardness (H) (GPa)	Contact Young's modulus E (GPa)
CSB	Chrome steel balls	2.00	62 ± 19	6.8	173 ± 11
LBS	Leighton Buzzard sand	1.18–2.36	223 ± 61	4.9	52 ± 12
LS	Crushed limestone	1.18–3.00	670 ± 221	1.2	16 ± 6
CDG	Completely decomposed granite	1.18–2.36	1341 ± 390	0.4[a]	7 ± 3

[a] Micro-hardness of CDG after Nardelli [47].

$$S_q = \sqrt{\frac{1}{uv}\sum_{ij} W_{ij}^2} \quad (1)$$

where u and v are the number of points in the horizontal plane (X and Y horizontal directions) and W is the deviation of each point from the mean height value (Z-direction). Typical images of flattened three-dimensional surface profiles of the geological materials (LBS, LS and CDG) are shown in Fig. 1 and the surface roughness values of the tested materials are listed in Table 1 expressed with an average value and a standard deviation for each material type. Typical scanning electron microscope (SEM) images of natural soil grains at different magnifications (100 and 6000x) are displayed in Fig. 2. It is observed in Fig. 2 that the LBS grain is relatively smoother compared to the other two geological materials. At a higher magnification, the calcite crystals can be identified on the LS grains. The presence of visible clayey coating is noticed on the surfaces of CDG, which, as described previously, is because of the weathering these grains have been subjected to. From Table 1, it can be observed that the average value and standard deviation of surface roughness for the CSB grains are very low (62 ± 19 nm). However, the surfaces of the natural materials are rougher in comparison to CSB (S_q equal to 223 ± 61 nm for LBS, 670 ± 221 nm for LS and 1,341 ± 390 nm for CDG).

The chemical composition of the tested materials was obtained through energy-dispersive X-ray spectroscopy (EDX) analysis. This technique is used to obtain the composition of constitutional elements in the material. The average composition of a set of grains from each material type is listed in Table 2. Silicon (Si), Oxygen (O), Aluminum (Al) and Iron (Fe) are the major elements present in LBS and CDG. Higher amount of combined Silicon (Si) and Oxygen (O) elements are present in LBS as they are the major constituents in forming Silicon dioxide. Calcium (C), Oxygen (O) and Carbon (C) are the major elements found in LS grains.

3. Experimental equipment and methods

Two major experimental methods were used in this study; one method was used to quantify the micro-hardness of the materials and a second one was used to quantify the force – displacement relationship and frictional behavior of the grains at their contacts. The micro-hardness of three of the tested materials (CSB, LBS and LS) was determined using the Fischer-scope HM2000 micro-hardness tester. The indenter is a standard Vickers diamond pyramid with an angle (β) of 136° between its faces. The indenter can apply a maximum normal force (F_N) of 2 N with a maximum indentation depth (h) of 150 μm.

For the normal and tangential force – displacement study, the custom built inter-particle loading apparatus described by Senetakis and Coop [61] and Nardelli [47], present at the City University of Hong Kong, was used. An image of the current version of the inter-particle loading apparatus is given in Fig. 3 displaying its various parts. The apparatus consists of a stainless-steel frame and three loading arms. Each arm consists of a linear micro-stepping motor, a high-resolution load cell of 100 N capacity and a precision of 0.02 N, and a non-contact eddy-current displacement sensor which has a resolution of 10^{-5}mm. The stainless-steel sled is placed on a bearing system of three chrome steel balls and a highly polished stainless-steel plate, allowing it to move across the horizontal plane with minimum friction. The horizontal arms are connected to the sled using various mechanical connections and linear micro-bearing systems. The particles are glued onto brass mounts of cylindrical cross section of 8 mm in diameter and 17 mm in height (shown in Fig. 4) and the mounts are placed into brass wells of a hollow cross-section located on the vertical loading arm (upper particle) and the stainless-steel sled (lower particle). The fixity of the mounts into the wells is achieved with laterally positioned screws. The apex-to-apex position of the grains is achieved by using two digital micro-cameras placed in two orthogonal horizontal directions as well as the monitoring of the reaction from the two horizontal load cells during the setting of the grains in contact. The whole apparatus is housed inside a Perspex chamber which helps in maintaining the humidity during the tests.

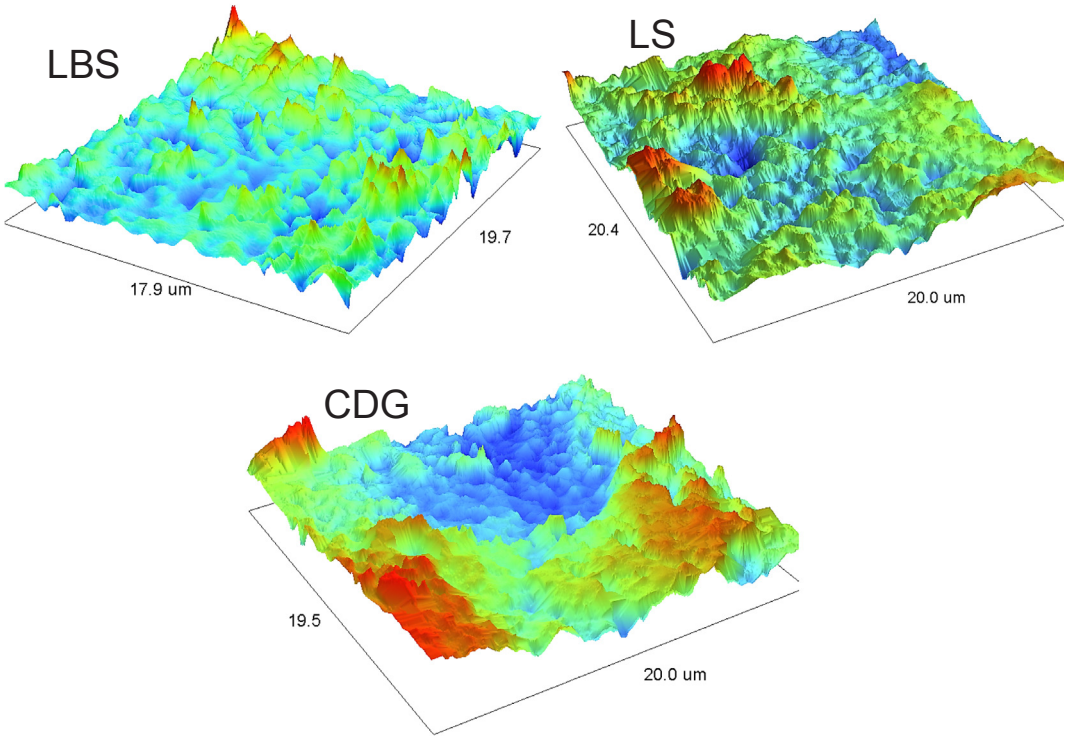

Fig. 1. Representative flattened three-dimensional surface profiles of soil grains (detected area of about 20 × 20 μm) based on interferometer analysis.

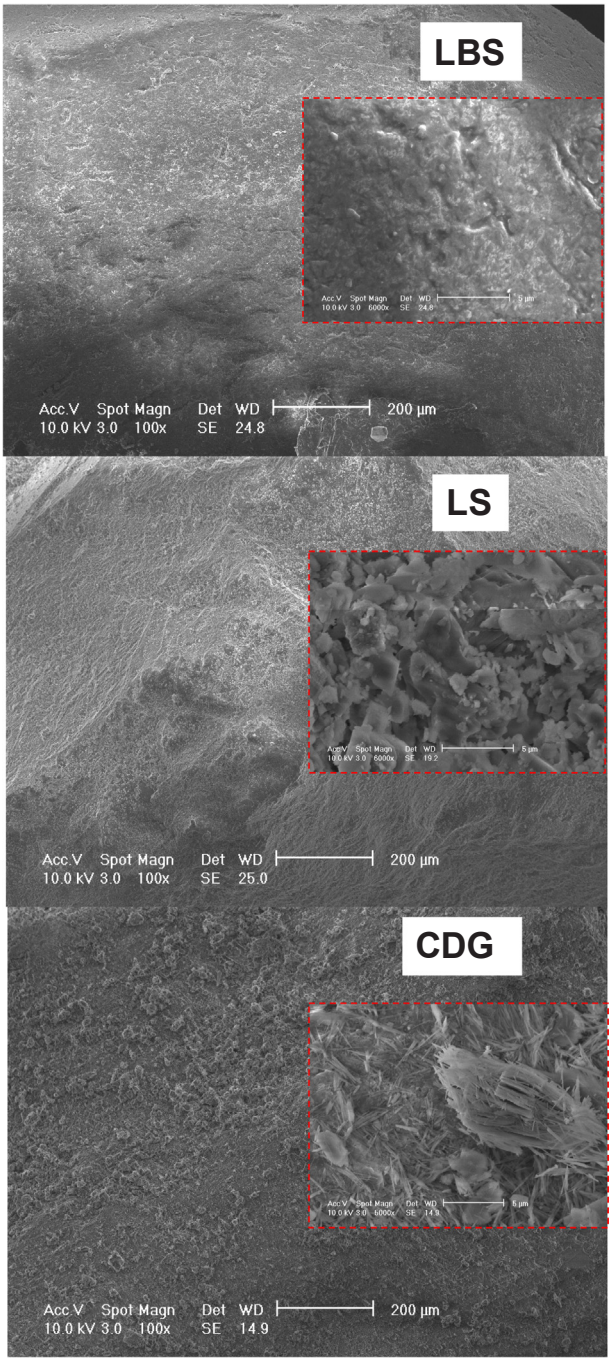

Fig. 2. Representative SEM images of soil grains at two different magnifications.

Table 2
Chemical composition through EDX analysis of the materials.

Element (%)	Material		
	LBS	LS	CDG
Si	46.5	–	26.2
O	42.4	35.5	47.7
Al	2.3	–	21.1
Fe	7.9	–	2.4
K	0.4	–	1.2
Mg	0.1	–	0.8
Ca	–	43.1	0.6
F	0.3	–	–
Mn	0.1	–	–
C	–	21.4	–

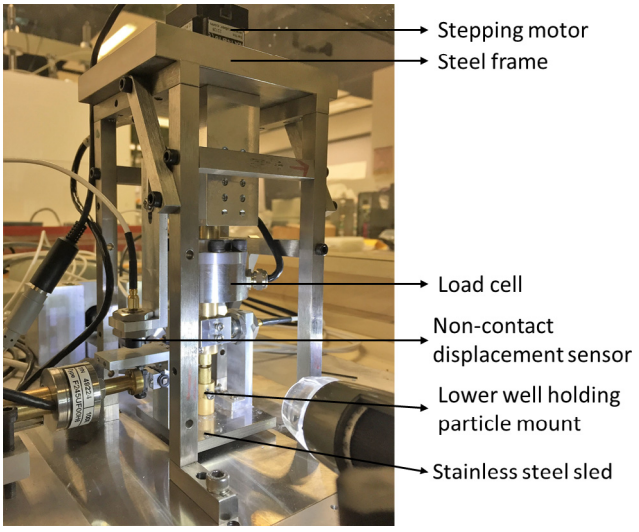

Fig. 3. Inter-particle loading apparatus.

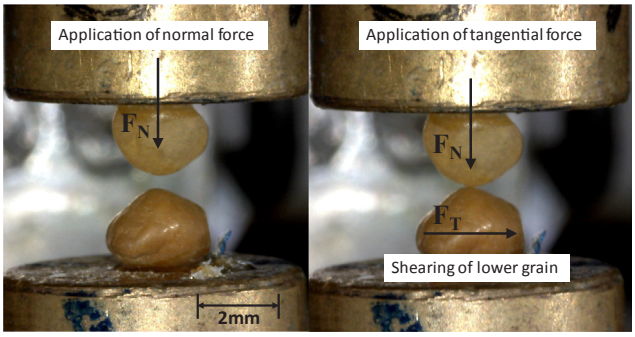

Fig. 4. Images of LBS grains during the application of normal and tangential force.

4. Major testing program

The major testing program consisted of sixteen inter-particle tests, which were conducted on four different pairs of grains from each material type and each test was conducted at a given normal force ranging from 1 to 8N under a displacement rate of 0.08 to 0.10 mm/h. These experiments are summarized in Table 3. The major testing program was used to develop expressions linking microslip displacement to the morphological and elastic characteristics of the grains. To understand any possible effect of the displacement rate on the inter-particle friction and slip displacement behavior, additional inter-particle shearing tests were conducted on LBS, with sliding velocities ranging from 0.03 to 0.3 mm/h. These experiments are summarized in Table 4. Additionally, four cyclic shearing tests were conducted on pairs of grains from LBS and LS in order to link the slip displacement of different material types with the energy losses during cyclic loading. These experiments, which are summarized in Table 5, were conducted at a displacement rate of 0.08–0.10 mm/h for a displacement amplitude of about 8 µm. A limited number of micro-hardness tests on six grains from CSB, LBS and LS were also conducted to determine the Martens hardness of the materials, while for CDG, micro-hardness values were taken from the literature [47]. Average values of the obtained hardness for the different materials are displayed in Table 1. The intention from the major testing program was to draw some general qualitative and quantitative conclusions with respect to the tangential load – displacement behavior of a broad range of granular materials including real soil grains. Each brand

Table 3
Major micro-mechanical testing program (shearing rate = 0.08–0.10 mm/h).

Material	Normal force (N)	Tangential force (N)	Inter-particle friction	$\delta_{T(\exp)}^{slip}$ (μm)	K_T^{2exp}	K_T^{2the}M-D
					(N/mm)	(N/mm)
CSB	1	0.10	0.10	1.2	81	2328
	2	0.25	0.13	2.3	140	2927
	5	0.60	0.12	3.8	254	4098
	8	0.67	0.08	2.4	580	4805
LBS	1	0.19	0.19	3.2	275	962
	2	0.24	0.12	3.8	204	1374
	5	0.96	0.19	6.0	400	1883
	7	1.80	0.26	11.0	380	2153
LS	1	0.28	0.28	3.6	225	468
	2	0.52	0.26	9.0	272	626
	3	1.00	0.33	11.5	333	639
	5	1.14	0.23	15.0	480	875
CDG	1	0.70	0.70	22.0	249	290
	2	0.59	0.30	10.8	326	362
	4	1.83	0.46	24.0	629	455
	5	2.65	0.53	32.0	580	498

*Note: Tangential force and inter-particle friction taken at the steady state or microslip condition.

Table 4
Micro-mechanical tests on LBS grains at different shearing velocities (F_N = 1 N).

Code	Shearing rate (mm/h)	Inter-particle friction	$\delta_{T(\exp)}^{slip}$ (μm)
LBS-0.3-1	0.3	0.16	6.2
LBS-0.3-2	0.3	0.38	7.1
LBS-0.1-3	0.1	0.25	7.5
LBS-0.1-4	0.1	0.29	3.6
LBS-0.03-5	0.03	0.35	6.0
LBS-0.03-6	0.03	0.18	4.8

Table 5
Energy loss based on cyclic shearing tests at a displacement amplitude of 0.008 ± 0.001 mm (shearing rate = 0.08–0.10 mm/h).

Material	Normal force (N)	ΔE (%)
LBS	1	61
LBS	5	30
LS	1	46
LS	5	19

of grains in the study had unique properties in terms of roughness, morphology of grains and elastic properties (as well as inter-particle friction). Even though the major testing program is relatively limited, the significant differences between the four material types can help to obtain some insights into the role of grain morphology (roughness in this case) and properties (contact Young's modulus and hardness) on their microslip displacement. Based on the developed expression from the major testing program, additional tests were re-analyzed in the study from previously published works, as it is described in subsequent sections, to verify the validity of the simple model proposed, particularly its stronger predictive capacity compared with available theoretical models. This can provide a rational basis for DEM modelers to simulate the force – displacement relationship of real soil grains to be used as input in discrete numerical analyses.

5. Results and discussion

5.1. Micro-hardness tests

Micro-hardness characterization was conducted on grains with similar morphological characteristics with the grains used for the inter-particle loading tests. During the experiments with the Fischer-scope HM2000 micro-hardness tester, the grain is held using a sample holder, which enables the apex of the particle to be at the same level with the holder. Polishing of the particles was avoided in this study as it could affect the residual stress state and the resultant hardness [21,68]. The micro-hardness tests were conducted in a force-controlled manner at a rate of 0.05 N/sec reaching the required normal force of 1 N. The micro-hardness values of the tested materials referring to Martens hardness (H), were calculated, based on Eqs. (2) and (3), as the ratio of the applied indentation force (F_N) to the surface area (A_S) of the indenter penetrating beyond the zero point of the contact (results are summarized in Table 1).

$$H = \frac{F_N}{A_S} \tag{2}$$

$$A_S = \frac{4h^2 \sin\left(\frac{\beta}{2}\right)}{\cos^2\left(\frac{\beta}{2}\right)} \tag{3}$$

The average value of the Martens hardness for CSB, LBS and LS were found equal to 6.8, 4.9 and 1.2 GPa, respectively, while the hardness values of CDG was equal to 0.4 GPa (after [47]). Todisco et al. [68] conducted micro-hardness tests by gluing the particles onto steel mounts using epoxy resin and they quantified the hardness only for the flat surfaces with average values of 6.2 and 1.6 GPa for LBS and LS particles, respectively. Daphalapurkar et al. [15] used the nano-indentation technique on polished surfaces of quartz sand and reported an average hardness value of 10.74 GPa. The hardness value from the previous study by Daphalapurkar et al. [15] is greater than the results on LBS, which is reasonable to be expected since the surfaces were polished and also the particular materials may have some differences with respect to their composition. It is also noticed that LBS grains have a greasy surface which has been reported to affect its frictional response [57]. However, the results by Todisco et al. [68] are reasonably close with respect to the current results since both studies ([68] and present paper) worked on LBS sand grains, even though these two studies deviated in the way that the hardness was measured (i.e. flat vs curved surfaces).

5.2. Normal contact behavior

Representative curves displaying the normal force (F_N) against normal displacement (δ_N) for the tested materials are shown in Fig. 5. It is observed that the F_N-δ_N relationship is non-linear and for most experiments, an initial plastic regime is observed, which has also been reported for geological and reference materials in previous studies (e.g. [5,47,56,57]). The great discrepancy in the observed responses between different pairs of grains in Fig. 5 is because of the different material types as well as their surface morphological properties. The Hertz model [29] is fitted to the experimental F_N-δ_N curves to quantify the contact (or apparent) Young's modulus and compare the results between the different grain types. This fitting is based on the following set of expressions ([29], after [40]):

$$\alpha = \left(\frac{3RF_N}{8E}\right)^{\frac{1}{3}} \tag{4}$$

$$\delta_N = 2\frac{\alpha^2}{R} \tag{5}$$

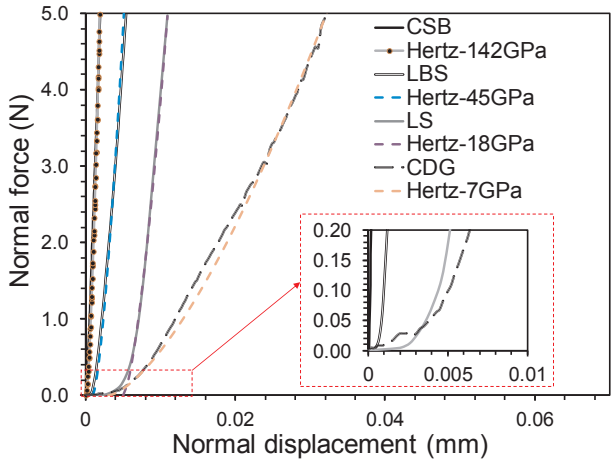

Fig. 5. Normal force against normal displacement for tested materials along with Hertzian fitting.

$$F_N = \frac{2\sqrt{2}\,(R)^{\frac{1}{2}}E^{*}\delta_N^{\frac{3}{2}}}{3} \tag{6}$$

$$\frac{1}{E^{*}} = 2\left[\frac{1-\nu^2}{E}\right] \tag{7}$$

where R is the radius of the spheres in contact taken as R = 1 mm in the study, since the grains had a diameter of approximately equal to 2 mm, α is the contact radius, E and ν correspond to the contact Young's modulus of the grains and the material Poisson's ratio, respectively, while E^{*} is the equivalent Young's modulus which was used to fit the theoretical (Hertzian) curves to the experimental data. Illustration of two ideal spheres in contact with explanation of the different parameters of the Hertzian fitting is shown in Fig. 6. It is noticed that the analysis of the normal force – displacement relationship of geological materials, which are not perfect spheres, with the Hertz model, can be conducted by means of local radius consideration. Sandeep and Senetakis [57] observed an increase of E of the order of 13–18%, when local radius was taken into account in comparison to Hertzian fitting using the average-approximate radius of the grains. However, in the same study it was reported that the consideration of average radius into the Hertz model, resulted in a satisfactory comparison between experimentally and theoretically obtained contact radii on LBS grains, compared with the consideration of local radius, at least for the range of small to medium normal forces.

Based on the Hertzian fitting, it is observed on the representative curves in Fig. 5 that the pair of grains from chrome steel balls had a contact Young's modulus (E) of 142 GPa, which is about three times greater than the observed E value for LBS. Among the three natural sands, LBS showed the stiffest response with a Young's modulus value of about 2.5 times greater than the crushed limestone grains and about 6.5 times greater in comparison to CDG. For the given set of material types (CSB, LBS, LS and CDG) and considering a total number of about ten tests for each type, Sandeep and Senetakis [56] reported that the most consistent results are observed for CSB, with a standard deviation of the order of 6% of the mean E value for these reference grains. Greater discrepancies are observed for geological materials, with a standard deviation of the order of 23%, 38% and 43% of the corresponding mean E value for LBS, LS and CDG, respectively.

In the above analysis as well as the reported results by Sandeep and Senetakis [56], the Poisson's ratio values used for the fitting of the Hertzian model were equal to 0.30 for CSB and LS and 0.25 for LBS and CDG, which values were assumed based on literature sources [32,72,22,18]. Fig. 7 provides a comparison of different resultant E values based on different assumptions of the Poisson's ratio for a given pair of grains of LBS, so that to understand the impact of the decision for (ν) value as input on the Hertzian fitting. It is shown that for a change of (ν) from 0.1 to 0.3, the resultant E decreases from about 55 to 51.5 GPa (change of the order of 6%), which implies that the effect of Poisson's ratio is markedly small in the Hertzian analysis of the normal force – displacement curves.

As mentioned before, most of the experimental F_N-δ_N curves showed an initial plastic response, which has also been reported as initial soft behavior in previous works. This initial plastic response is observed to be very small for CSB, within a range of about 0.05–0.15 μm of normal displacement, but it becomes noticeable for the geological materials. It is meant that the Hertzian fitting is in general applicable beyond the threshold displacement of the occurred initial plastic response. Typical boundary values of this threshold displacement are displayed in Table 6 for the different material types of the study. For LBS, this range is between about 0.35 and 0.90 μm, which means that there is an initial soft behavior and beyond normal displacements of about half to one micron, Hertzian fitting is applicable. However for the much rougher and softer grains of LS and CDG, the application of the Hertzian fitting was valid beyond about 1–2 μm or even beyond 10 μm for some of the experiments. This initial soft response has been attributed to plastic deformation of asperities, so that grains of very rough surfaces or lower stiffness display extended threshold displacements between plastic regime and Hertzian response [5,11,56,57]. Cole and Hopkins [11] mentioned that this behavior is due to the domination of asperity contact initially, which asperities are then flatted giving rise to nearly smooth contact which turns the normal contact response to fit the Hertzian model. The important role of roughness on the normal contact behavior of materials has also been acknowledged in earlier studies by Greenwood and Tripp [19] and Kendall [42].

5.3. Tangential contact behavior

Fig. 8 gives the general representation of tangential force against displacement behavior at the contact of grains during shearing, where two major regions can be observed based on Eq. (8) [46,51,71,2].

$$F_T < \mu F_N \tag{8}$$

The first region expresses a non-linear increase of tangential force

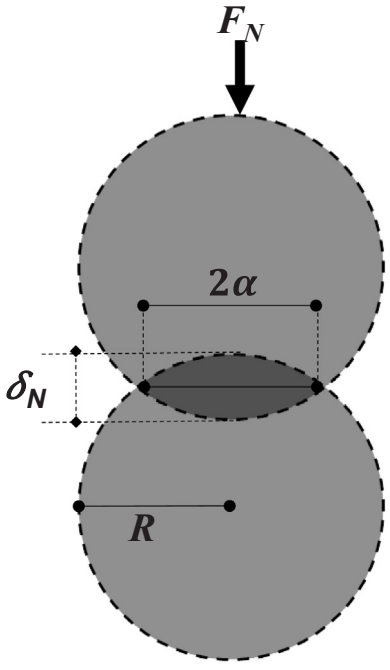

Fig. 6. Sketch of ideal spheres in contact.

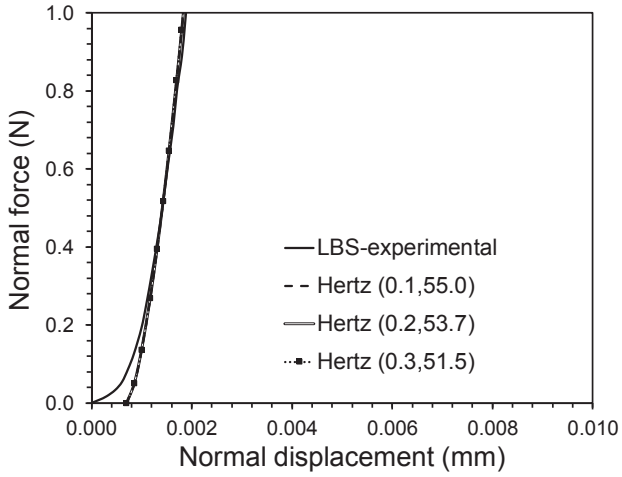

Fig. 7. Normal force against normal displacement behavior of LBS with Hertzian fitting considering different Poisson's ratio values (first number in parenthesis denotes Poisson's ratio and second number denotes contact Young's modulus in GPa).

Table 6
Normal displacements corresponding to the application of Hertzian fitting.

Material	Normal displacement range (μm)	
	Min	Max
CSB	0.05	0.15
LBS	0.35	0.90
LS	1.00	8.00
CDG	2.00	12.00

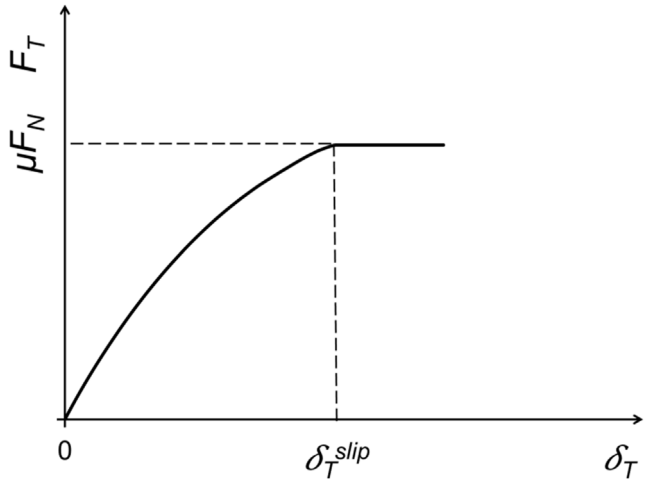

Fig. 8. Schematic plot of tangential force against tangential displacement illustrating the slip displacement.

with the increase in displacement, whereas the second regime expresses a plastic region where the tangential force remains constant at increasing displacements. As depicted in Fig. 8, these two regimes are separated by a threshold displacement, which is termed as the slip (or microslip) displacement denoted in the study as δ_T^{slip}. This threshold displacement occurs when the tangential force reaches the product of inter-particle friction and applied normal force. Theoretically, this means that for a given material type, δ_T^{slip} depends on both the normal force as well as the inter-particle coefficient of friction of the contacted surfaces so that it is expected that surface roughness and Young's modulus of the contacted grains will also play a role in the definition of

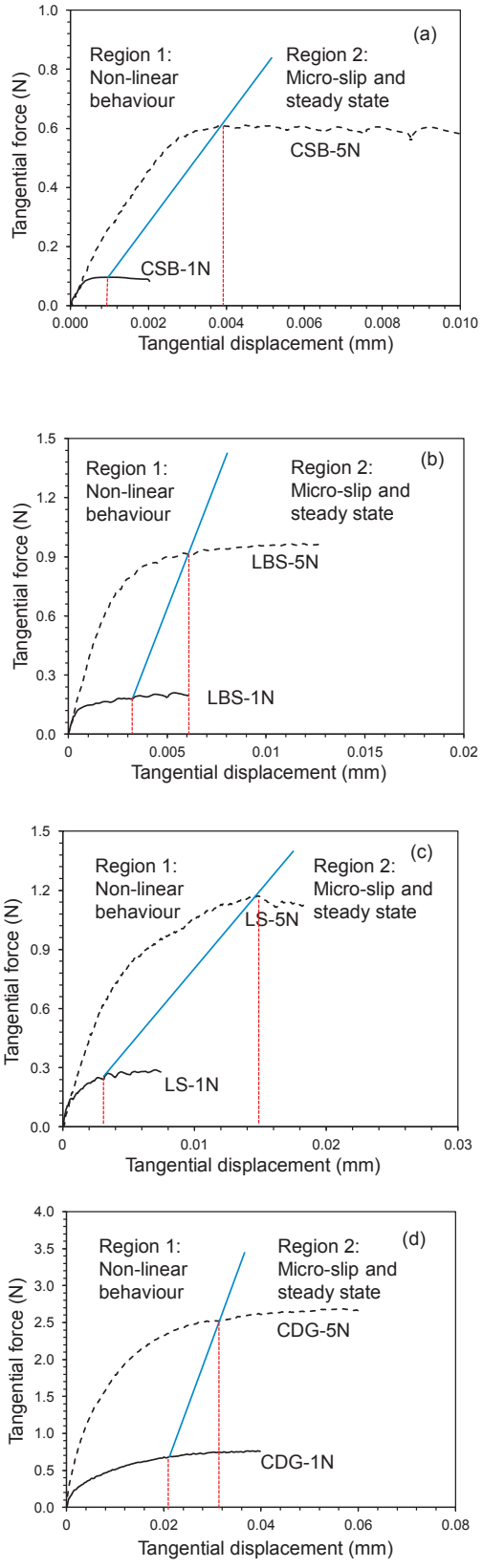

Fig. 9. Tangential force against tangential displacement for various materials showing different regions (a) CSB (b) LBS (c) LS (d) CDG.

this threshold displacement.

Representative micromechanical shearing test results on the different geological materials and CSB are shown in Fig. 9(a)–(d), which results correspond, for each material type, to a normal force of 1 and 5 N. A comparison of the different material types in terms of tangential force – displacement curves at $F_N = 5$ N is given in Fig. 10. Similar to the theoretical illustration in Fig. 8, the experimental results in terms of tangential force against displacement for the different material types, show two distinct regions of behavior in agreement as well with previous studies on contacted engineered and naturally occurred geological surfaces [49,57]. In region 1, the response is non-linear and the tangential force increases with displacement showing gradual stiffness reduction. In region 2, microslip/steady state can be observed after the tangential stiffness reaches zero. The microslip is due to the continuous break down of the contacting asperities even beyond the slip displacement. In some of the curves from Figs. 9 and 10, a microslip condition is observed rather than a clear steady state. Previous works on geological materials (e.g. [12,56,57] have observed the similar behavior; this has been attributed to the brittle nature of the contacting asperities as well as to morphology effects of the grain surfaces. Two major observations in the experimental results of Figs. 9 and 10 are that for a given material type, the slip displacement increases at greater normal forces and for a given normal force, materials of greater roughness and lower Young's modulus, which also display greater inter-particle friction, exhibit extended slip displacements. Fig. 11 shows representative plots in terms of tangential stiffness (K_T) against tangential displacement (δ_T) at 1 and 5 N of normal force. The tangential stiffness is obtained by differentiating the tangential force over the displacement for a set of about six to twelve data points (similar to [62]). These results emphasize the highly non-linear response of both reference and natural grains and that beyond displacements of the order of about 2–20 μm, K_T reaches zero. It is acknowledged however, as expected from the results in Figs. 9 and 10, that for the chrome steel balls, which have the smoothest and stiffest surfaces, the tangential stiffness degrades faster in comparison to the geological materials, while, among the different geological materials, the most rough and soft grains of CDG display the greatest displacements beyond which K_T is zeroed.

In Table 3, the experimental results are summarized in terms of tangential force at the steady state (or microslip) condition, the resultant inter-particle coefficient of friction as well as the slip displacement. Combining the results as displayed in Table 3 and Figs. 9–11, it is observed that materials of greater inter-particle friction and lower stiffness have greater slip displacements. Thus, the initial assumption that surface roughness and contact Young's modulus influence the observed slip displacements is confirmed from the experimental results. These parameters including the inter-particle coefficient of friction, the tangential and normal contact stiffnesses as well as the slip displacement are key input properties in DEM analyses controlling, for example, the macro-scale behavior of granular materials subjected to monotonic or cyclic loading, or the flowability of soil mass movements which is important in granular flow simulations (e.g. [59,30,71]).

The experimental results of six different shearing tests on LBS pairs of grains subjected to a normal force of 1 N and variable velocities are summarized in Table 4 and representative tangential force – displacement curves are plotted in Fig. 12. In general, for the relatively narrow range of velocities applied in the study, between 0.03 and 0.3 mm/h, there was not observed a clear effect of the sliding velocity on the inter-particle coefficient of friction. In terms of slip displacement, within the scatter of the data, it was observed a slight shift of δ_T^{slip} to greater displacements for the pairs of grains tested at higher velocities, considering averaged values of δ_T^{slip} for each set of two grains tested at 0.03, 0.1 and 0.3 mm/h. However, the results in Table 4 imply that a wider range of velocities is necessary to be applied in order to obtain firm conclusions with respect to the influence of shearing velocity on the microslip displacement.

5.4. Comparison with analytical models

Mindlin and Deresiewicz [46] referred to as M-D, proposed a theory to study the contact problem of two elastic spheres in contact, where the initial part of the tangential force against displacement curve is non-linear and it is followed by purely plastic behavior (Fig. 8). They proposed Eqs. (9) and (10) to obtain the initial tangential stiffness (K_T^0) and the tangential stiffness at any displacement (K_T^x):

$$K_T^0 = 4\alpha\left(\frac{G}{2-\nu}\right) \tag{9}$$

$$K_T^x = K_T^0\left(1 - \frac{F_T^x}{\mu F_N}\right)^{\frac{1}{3}} \tag{10}$$

where G is the shear modulus of the materials in contact, and F_T^x is the tangential force at any displacement x. The value of K_T^x reaches zero when the value of F_T^x equals to the product of the inter-particle friction (μ) and the applied normal force (F_N) (Fig. 8). A comparison between experimental and theoretical M-D tangential force displacement curves is given in Fig. 13 for a test on LS pair of grains. The theoretical curve poorly fits the experimental data which might be, partly, due to the differences in the predicted stiffness (K_T) degradation rate as the M-D model predicts that the stiffness degradation follows a power of 1/3 (Eq.(10)), which is independent on material type. Table 3 gives a summary of the experimentally obtained values of stiffness (defined at a tangential displacement of 2×10^{-4} mm) denoted as K_T^{2exp} for all the pairs of grains, which is termed as the initial tangential stiffness in the study, as well as the corresponding theoretical stiffnesses, denoted as K_T^{2the}, which are obtained based on Eq. (10).

Olsson and Larsson [51] referred as O-L, presented an elastic-plastic model by assuming isotropic power law hardening behavior for different materials with varying yield stresses including large deformations. Using a finite element code, they modified the M-D expression of Eq. (9) for the initial tangential stiffness to Eq. (11) by accounting for the transition from stick to slip of the contact.

$$K_T^0 = 4\alpha\left(\frac{G}{2-\nu}\right)\left(1 - 1.54\frac{\alpha}{R}\right) \tag{11}$$

Fig. 14 gives a comparison between experimental K_T^{2exp} and theoretical K_T^{2the} stiffnesses (using both M-D and O-L models) for the LBS and LS pairs of grains displaying these stiffnesses against the normal force. A first important comment on the data in Fig. 14 is that the

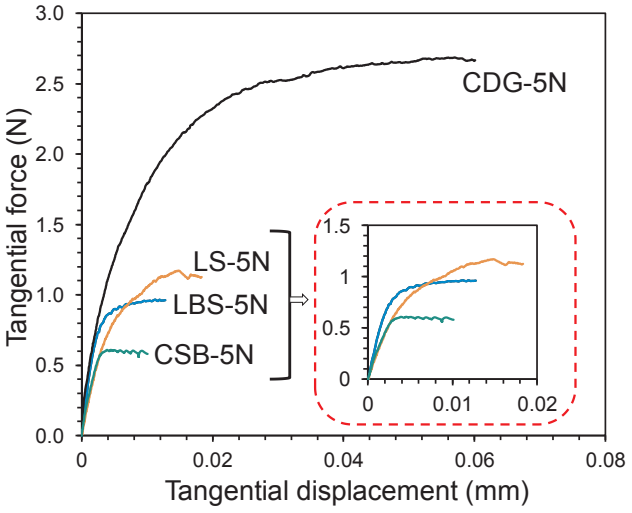

Fig. 10. Tangential force against displacement of tested materials when sheared at 5 N of normal force.

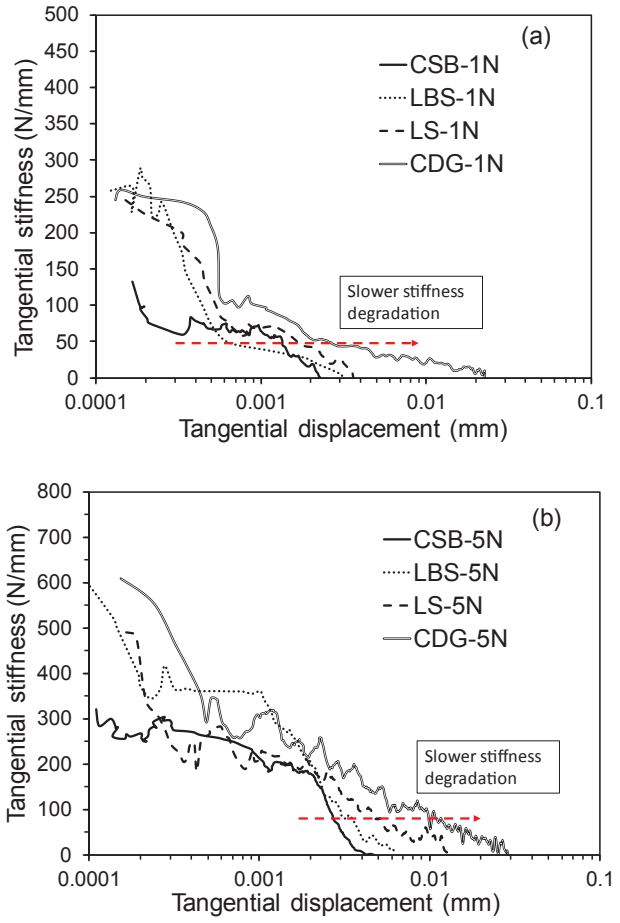

Fig. 11. Tangential stiffness degradation curves for the materials tested at (a) 1 N and (b) 5 N of normal force.

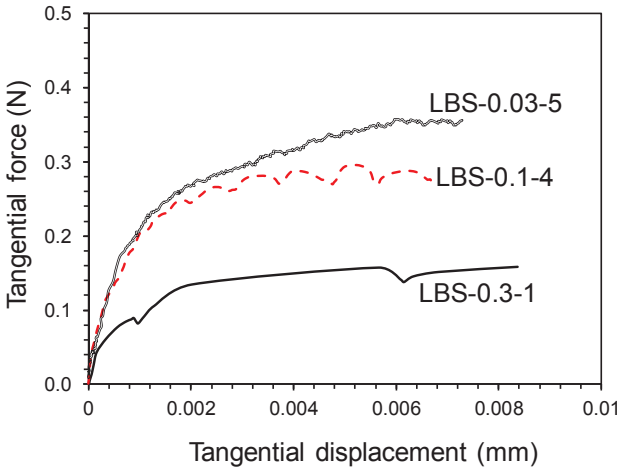

Fig. 12. Tangential force against displacement curves for LBS grains at different shearing rates.

experimental (as well as the theoretical) tangential stiffness increases with the increase in normal force for both LBS and LS. It is also observed that both the M-D and O-L models over-predict the experimental tangential stiffness. Combining the results shown in Fig. 14 and Table 3, it is concluded that the theoretical models over-predict the initial stiffness of the CSB, LBS and LS, but there is a clear convergent between experimental and theoretical values, based on the M-D model, for CDG

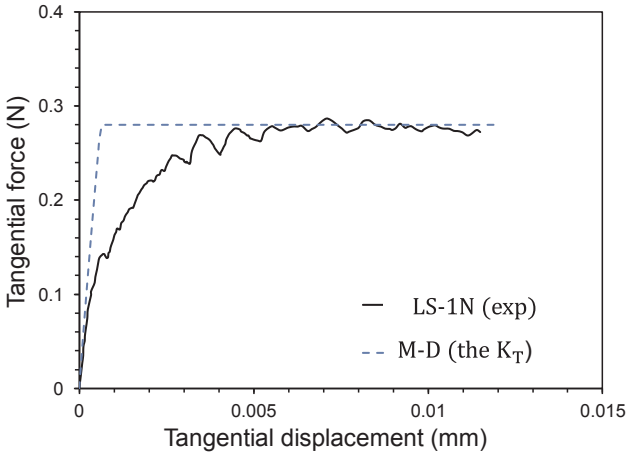

Fig. 13. Comparison between experimental and theoretical (M-D) tangential force against displacement curve for LS at 1 N of normal force.

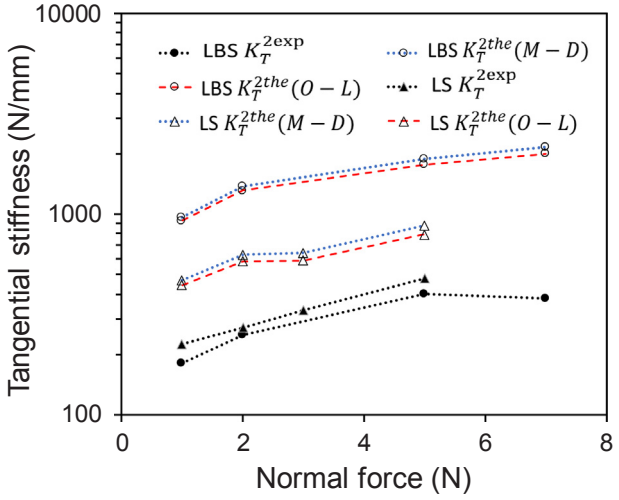

Fig. 14. Comparison between experimentally and theoretically (M-D and O-L models) obtained tangential stiffness defined at 0.0002 mm of displacement.

pairs of grains. In particular, for LBS, which display the greatest Young's modulus among the geological materials, the M-D model over-predicts about 3.5 to 7 times the initial tangential stiffness. For LS, which display lower Young's modulus (a well as greater roughness) in comparison to LBS, the M-D model over-predicts about 2 times the experimentally derived stiffness, while for the CDG pairs of grains, which have the lowest Young's modulus (as well as the highest roughness) among the geological materials in the study, there is a satisfactory comparison between experiment and theory. It is also observed in Fig. 14 that the O-L model gives systematically slightly lower values of stiffness, compared to the M-D model, of the order of about 3–13%.

Mindlin and Deresiewicz [46] proposed an expression to calculate the slip displacement as shown in Eq. (12) as a function of the Poisson's ratio and the contact shear modulus of the material, the inter-particle coefficient of friction, the normal force and the radius of contact:

$$\delta_{T(the)}^{slip} = \frac{3(2-\nu)\mu F_N}{16G\alpha} \tag{12}$$

where $\delta_{T(\text{the})}^{slip}$ is the theoretically obtained slip displacement based on the M-D model.

Based on the application of the Hertzian fitting, which was discussed in Section 5.2, and the derived values of contact radius (α) and contact shear modulus (G), a comparison between the theoretically

predicted slip displacements, based on Eq. (12), and experimentally obtained values for LBS and LS, is given in Fig. 15. It is observed that a poor agreement exists between theoretical and experimentally measured slip displacements for the geological materials. For the examples in Fig. 15, there is a difference of one order of magnitude and beyond that between theoretically predicted and measured slip displacements for LBS and LS grains.

It is noticed that the elastic-plastic model by Olsson and Larsson [51] accounts for the hardness of the material and it was built, to predict the slip displacement, based on powder compaction. However, the ratio of slip displacement to the area of contact in the present study (with a range of values of 0.07–0.38) is in general much greater than the values considered by Olsson and Larsson [51] model (with a range of 0–0.08). Hence, in the subsequent section where a simple expression will be presented for the slip displacement of geological materials, the model proposed by Olsson and Larsson [51] is not discussed further, but the analysis will consider the M-D theory. However, the modification of the M-D model will incorporate the concept of hardness which is part of the Olsson and Larsson [51] theory.

5.5. Slip displacement equation incorporating normalized hardness

Even though the M-D slip displacement (Eq. (12)) did not account for hardness, Mindlin and Deresiewicz [46] considered inter-particle friction in their model to obtain slip displacements. The M-D slip displacement (Eq. (12)) is modified in the present study by normalizing the hardness of the materials using Eq (13) under the assumption that Martens hardness is linearly related to yield stress [39,40,4,51].

$$H_N = \frac{F_N}{\alpha H} \tag{13}$$

In Eq. (13), H_N is the normalized hardness and H is the Martens hardness (Table 1). It is noted that the term on the right side corresponds per unit length (i.e. it is implied that the ratio is divided by 1 mm) so that H_N on the left side of Eq. (13) is presented in a dimensionless form.

Fig. 16(a) shows the relationship between the slip displacement ratio $\delta^{slip}_{T(\exp)}/\delta^{slip}_{T(\text{the})}$ and H_N. Within the scatter of the data, it is observed that the decrease of the slip displacement ratio follows a power law with the increase in normalized hardness (with a power of -0.51). Hence, the experimental slip displacement can be expressed as a function of the theoretical slip displacement (Eq. (12)) and the normalized hardness. The relationship between experimental and theoretical slip displacement (M-D) with varying hardness for the different materials tested in this study in given in Fig. 16(b) and Eq. (14), which can be re-written as Eq. (15).

$$\delta^{slip}_{T(\exp)} = \frac{3\delta^{slip}_{T(the)}}{\sqrt{H_N}} \tag{14}$$

$$\delta^{slip}_{T(\exp)} = \frac{9(2-\nu)\mu F_N}{16G\alpha\sqrt{H_N}} \tag{15}$$

Fig. 15 shows the comparison between slip displacement obtained experimentally, theoretically (M-D) and from the new expression in Eq. (15). It is observed that the modified expression (i.e. modification of M-D model accounting for the normalized hardness) satisfactorily predicts the slip displacement values when compared to the M-D theoretical slip displacement (Eq. (12)). Sandeep and Senetakis [56] showed that the inter-particle friction of the natural materials can be related to roughness and Young's modulus. Hence, the above modified expression in Eq. (15), gives the slip displacement for different material properties, roughness and hardness when the grains are sheared under different normal forces. All these parameters used in Eq. (15) can be obtained by relatively simple experimental techniques and the application of the Hertz theory.

To check the validity of Eq. (15), experimental slip displacement values against predicted values are plotted in Fig. 17 for twenty-five independent tests (value of F_N ranges between 1 and 15 N) and for four different materials from previously reported data: LBS, beach sand (BS), river sand (RS), and CSB (after [58,55]). Properties of the materials which are used for the comparison with the newly proposed expression are listed in Table 7 and Table 1(for LBS grains). Note that this new set of data points on LBS used in Fig. 17 was not included in the development of the new expression in Eq.(15). Considering that for a given natural material, variations are observed from grain to grain with respect to morphology, roughness and elastic properties as well as inter-particle friction, it can be seen that the comparison of theoretical values from Eq. (15) and independent experimental data in Fig. 17 is satisfactory with most data falling within a range of ± 30% in terms of predictive capacity. The scatter of ± 30% implies a reasonable prediction, for example, for a real slip displacement of 2 μm (this value would be representative for CSB as well as for LBS at very low normal forces), the estimated slip displacement from Eq. (15) might range from 1.4 to 2.6 μm, while for a real slip displacement of 30 μm (this value would be representative for CDG), the estimated slip displacement might range between 21 and 39 μm. Thus, the newly proposed expression provides a much better prediction of the experimental data compared with the theoretical models (M-D, O-L), which predict values one order of magnitude different or beyond that, compared with the experimental data as discussed previously. Therefore, the use of Eq. (15) can be considered as a first rational step to be utilized in DEM simulations

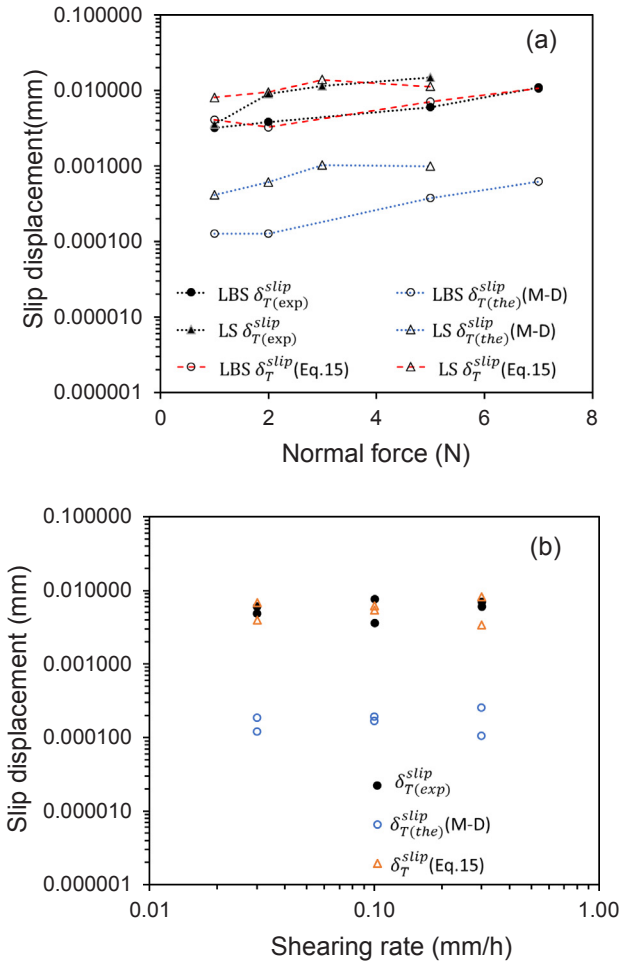

Fig. 15. Comparison between experimental, theoretical (M-D) and modified (Eq. (15) of present study) slip displacement (a) for LBS and LS grains at different normal forces (b) for LBS grains at different shearing rates (F_N = 1 N).

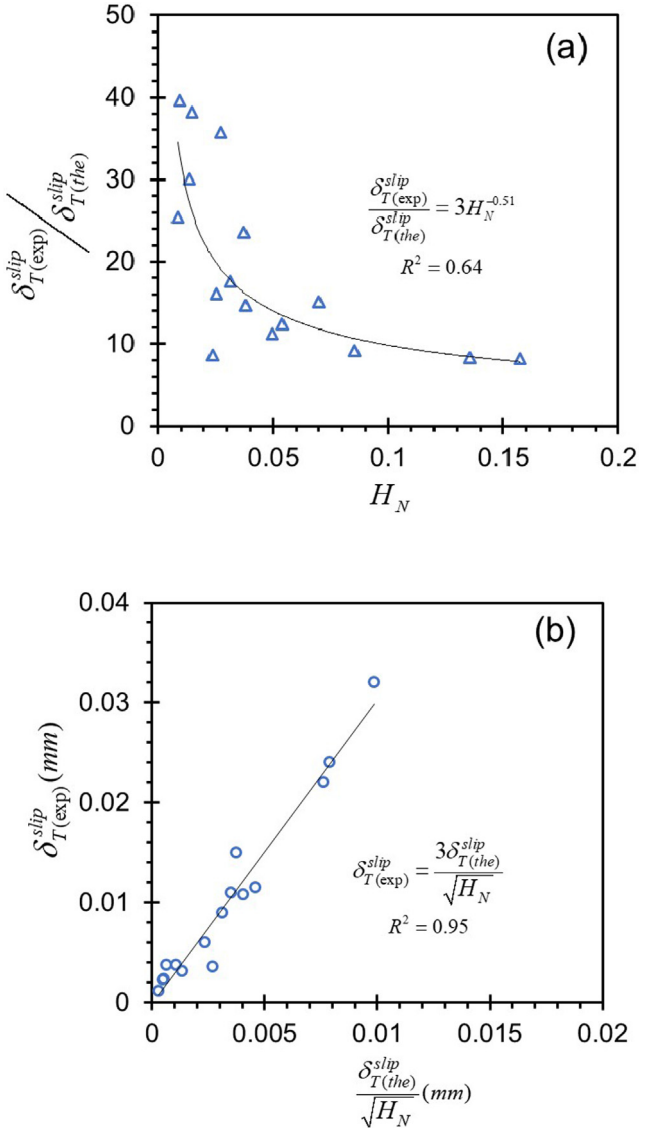

Fig. 16. Relationship between experimental and theoretical slip displacement (M-D) as a function of normalized material hardness.

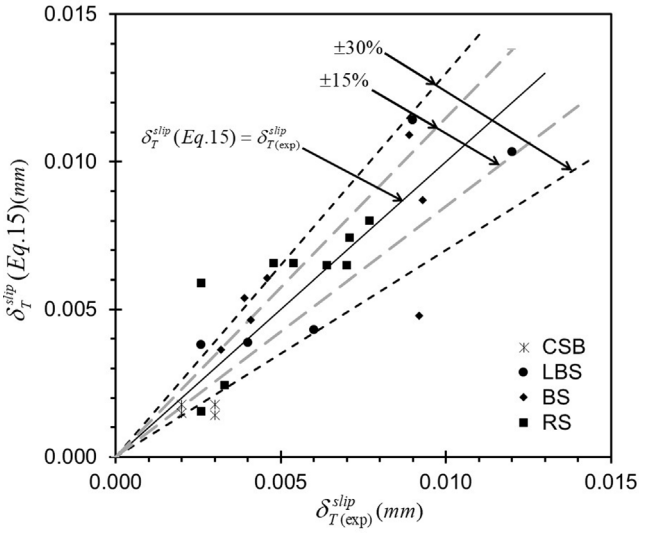

Fig. 17. Comparison between experimental and predicted slip displacement values based on a set of independent micromechanical tests.

compared with available models.

The slip displacement can be used to understand (or interpret) the damping and energy loss behavior at the contacts of geological materials. To this extent, a limited number of cyclic shearing tests was conducted on LBS and LS grains similar to Sandeep and Senetakis [57] and Sandeep et al. [54] at a displacement amplitude of about 0.008 mm under the application of 1 and 5 N of normal force and the results are displayed in Fig. 18. The energy loss percentage (ΔE) was calculated in the study from the area of the closed loop (ΔL) which corresponded to the second shearing cycle and the elastic energy stored (L) from Eq. (16). The results are summarized in Table 5.

$$\Delta E = \frac{100\Delta L}{4\pi L} \tag{16}$$

Based on Table 5 and considering a given magnitude of normal force, the energy loss is greater for LBS compared to LS grains. For both materials, the energy loss was found to be greater at a normal force of 1 N compared to 5 N. This behavior can be attributed to the lower values of slip displacement for LBS compared to LS grains as well as to the increase of the slip displacement at greater normal forces.

6. Conclusions

The micromechanical behavior of different materials which included reference chrome steel balls (CSB) as well as three natural-geological materials was investigated in terms of normal/tangential contact behavior and inter-particle friction, with particular focus on the slip displacement and its relationship with material properties. Additionally, micro-hardness experiments were conducted to evaluate the Martens hardness of the geological and reference materials. The characterization of the grains showed that the particles from completely decomposed granite (CDG) had the greatest values of roughness as well as the lowest hardness compared with the other types of grains. At initial stages of normal displacements, soft response was observed during normal loading, which was ascribed to asperity behavior. The initial soft behavior was more pronounced for the geological materials compared to the reference grains, particularly for those having greater roughness. Hertz [29] theory was used to fit the normal force against displacement curves to obtain contact Young's modulus (E). The reference grains showed the highest values of E, while Leighton Buzzard sand quartz grains (LBS) had greater E values among the geological materials. Additionally, crushed limestone grains (LS) displayed greater E values compared to CDG.

From the shearing tests, two different regions were observed in the tangential force - displacement curves. The response was initially non-linear, followed by a steady-state or microslip condition. The rate of shearing, within the relatively limited range of velocities applied in the study from 0.03 to 0.3 mm/h, did not produce observable differences in the frictional response of LBS, but, within the scatter of the data, averaged values of slip displacement showed a very slight increase with the increase of the shearing velocity.

Two theoretical models were applied, named the Mindlin and Deresiewicz [46] (termed as M-D model) and the elastic-plastic model by Olsson and Larsson [51] (termed as O-L model) to further explore the differences between theory and experiment in terms of tangential stiffness and slip displacement. It was shown that both M-D and O-L models over-predicted the tangential stiffness of the materials in the study apart from the softer and rougher CDG grains, for which, the M-D model demonstrated a satisfactory prediction. Similar to these observations, the M-D model over-predicted the slip displacements (i.e. the threshold displacement to reach a zero stiffness) for the materials in the study, which over-prediction was of one order in magnitude or beyond. A modification of the M-D expression was applied accounting for the material hardness, which was incorporated as a normalized value so that a modified expression was proposed which could satisfactorily predict the slip displacement of the geological materials.

Table 7
Properties of the materials used for comparison.

Material code	Material description	Diameter (mm)	Surface roughness (S_q) (nm)	Hardness (H) (GPa)	Contact Young's modulus E (GPa)
CSB	chrome steel balls	5.00	48 ± 22	6.8	176 ± 14
BS	beach sand	1.18–2.50	293 ± 56	4.9	44 ± 16
RS	river sand	1.18–2.50	195 ± 30	4.9	48 ± 11

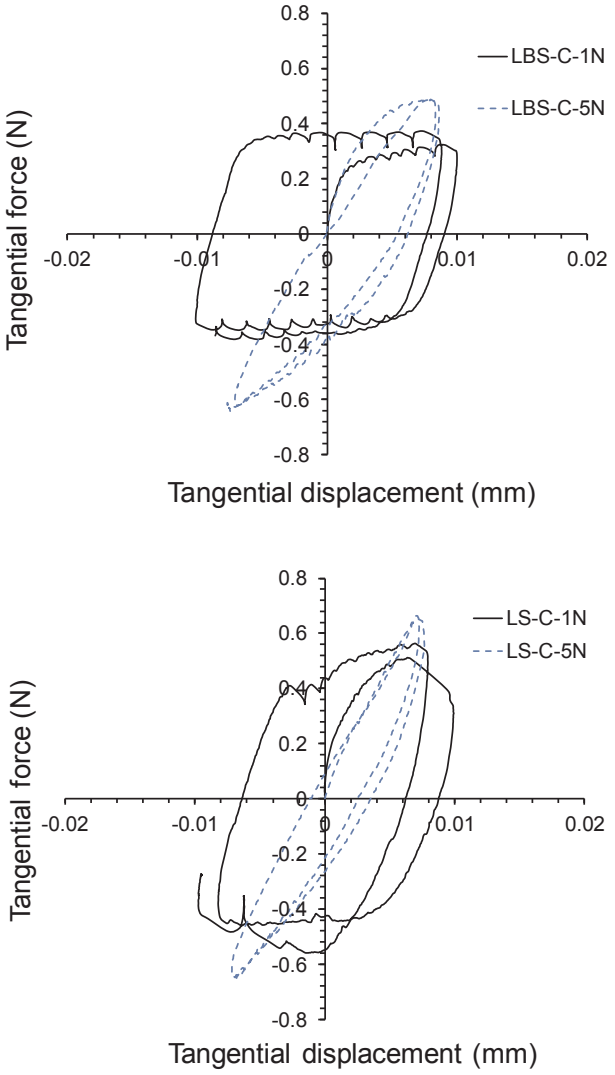

Fig. 18. Cyclic shearing tests on LBS and LS grains at 1 and 5 N of normal force.

Validation of the new expression was performed comparing the slip displacements with experimental data from previous studies on a broad range of granular materials. Within the scatter of the data, it was shown that the comparison between theoretical and experimental values was much better when the new expression for slip displacement was used compared with the use of available models.

Acknowledgments

The authors appreciate the constructive comments and suggestions made by the reviewers to improve the quality of the manuscript. The authors acknowledge the grants from the Research Grants Council of the Hong Kong Special Administrative Region, China, project no. "T22-603/15N" and project no. "CityU 11206617". The technicians of the City University Mr Thomas Tsang and Mr Kian are acknowledged for their continuous contribution and help in the lab facilities development and maintenance.

References

[1] Asaf Z, Rubinstein D, Shmulevich I. Determination of discrete element model parameters required for soil tillage. Soil Tillage Res 2007;92(1–2):227–42.
[2] Balevičius R, Mróz Z. Modeling of combined slip and finite sliding at spherical grain contacts. Granular Matter 2018;20(1):10.
[3] Brizmer V, Kligerman Y, Etsion I. Elastic–plastic spherical contact under combined normal and tangential loading in full stick. Tribol Lett 2007;25(1):61–70.
[4] Busby JT, Hash MC, Was GS. The relationship between hardness and yield stress in irradiated austenitic and ferritic steels. J Nucl Mater 2005;336(2–3):267–78.
[5] Cavarretta I, Coop MR, O' Sullivan C. The influence of particle characteristics on the behavior of coarse grained soils. Geotechnique 2010;60(6):413–23.
[6] Cavarretta I, Rocchi I, Coop MR. A new interparticle friction apparatus for granular materials. Can Geotech J 2011;48(12):1829–40.
[7] Chen W, Deng X. Structural damping caused by micro-slip along frictional interfaces. Int J Mech Sci 2005;47(8):1191–211.
[8] Cheung LYG, O'Sullivan C, Coop MR. Discrete element method simulations of analogue reservoir sandstones. Int J Rock Mech Min Sci 2013;63:93–103.
[9] Coetzee CJ. Calibration of the discrete element method. Powder Technol 2017;310:104–42.
[10] Cole DM. Laboratory observations of frictional sliding of individual contacts in geologic materials. Granular Matter 2015;17(1):95–110.
[11] Cole DM, Hopkins MA. The contact properties of naturally occurring geologic materials: experimental observations. Granular Matter 2016;18(3):62.
[12] Cole DM, Mathisen LU, Hopkins MA, Knapp BR. Normal and sliding contact experiments on gneiss. Granular Matter 2010;12(1):69–86.
[13] Conroy M, Mansfield D. Scanning interferometry: measuring microscale devices. Nat Photonics 2008;2(11):661.
[14] Cundall PA, Strack OD. A discrete numerical model for granular assemblies. Geotechnique 1979;29(1):47–65.
[15] Daphalapurkar NP, Wang F, Fu B, Lu H, Komanduri R. Determination of mechanical properties of sand grains by nanoindentation. Exp Mech 2011;51(5):719–28.
[16] Desai CS, Drumm EC, Zaman MM. Cyclic testing and modeling of interfaces. J Geotech Eng 1985;111(6):793–815.
[17] Duan K, Kwok CY. Discrete element modeling of inherently anisotropic rock under Brazilian test conditions. Int J Rock Mech Min Sci 2015;78:46–56.
[18] Gill WS, Marshall MB, Lewis R, Hall B, Bolton S. Failure analysis of pipeline indents using steel precision balls under subsea conditions. Tribol Int 2018;118:524–37.
[19] Greenwood JA, Tripp JH. The elastic contact of rough spheres. J Appl Mech 1967;34(1):153–9.
[20] Greenwood JA. Problems with surface roughness. In: Singer IL, Pollock H, editors. Fundamentals of friction: macroscopic and microscopic processes. Dordrecht, The Netherlands: Kluwer Academic Publisher; 1992.
[21] Griepentrog M, Ullner C, Duck A. Instrumented indentation test for hardness and materials parameter from millinewtons to kilonewtons. VDI BERICHTE 2002;1685:105–12.
[22] Gu XQ, Yang J. A discrete element analysis of elastic properties of granular materials. Granular Matter 2013;15(2):139–47.
[23] Guo N, Zhao J. A coupled FEM/DEM approach for hierarchical multiscale modelling of granular media. Int J Numer Meth Eng 2014;99(11):789–818.
[24] Guo N, Zhao JD. 3D multiscale modeling of strain localization in granular media. Comput Geotech 2016;80:360–72.
[25] Guo N, Zhao JD. Multiscale insights into classical geomechanics problems. Int J Numer Anal Meth Geomech 2016;40(3):367–90.
[26] Hanaor DAH, Gan Y, Einav I. Contact mechanics of fractal surfaces by spline assisted discretisation. Int J Solids Struct 2015;59:121–31.
[27] Hanaor DAH, Gan Y, Einav I. Static friction at fractal interfaces. Tribol Int 2016;93:229–38.
[28] Hanaor DAH, Gan Y, Einav I. Effects of surface structure deformation on static friction at fractal interfaces. Geotech Lett 2013;3:52–8.
[29] Hertz H. Uber die Beruhrang fester elastischer Korper (On the contact of elastic solids). Journal für die reine und angewandte Mathematik 1882;92:156–71.
[30] Huang X, Hanley KJ, O'Sullivan C, Kwok CY. Exploring the influence of inter-particle friction on critical state behaviour using DEM. Int J Numer Anal Meth Geomech 2014;38(12):1276–97.
[31] Huang X, Hanley KJ, O'Sullivan C, Kwok CY. Implementation of a rotational resistance models: a critical appraisal. Particuology 2017;34:14–23.
[32] Irfan TY, Dearman WR. Engineering classification and index properties of a weathered granite. Bull Eng Geol Environ 1978;17(1):79–90.
[33] Iverson RM, Reid ME, Logan M, LaHusen RG, Godt JW, Griswold JP. Positive feedback and momentum growth during debris-flow entrainment of wet bed sediment. Nat Geosci 2011;4(2):116.

[34] Jiang MJ, Yu HS, Harris D. Discrete element modelling of deep penetration in granular soils. Int J Numer Anal Meth Geomech 2006;30(4):335–61.
[35] Jiang M, Fu C, Cui L, Shen Z, Zhu F. DEM simulations of methane hydrate exploitation by thermal recovery and depressurization methods. Comput Geotech 2016;80:410–26.
[36] Jiang M, Zhu F, Utili S. Investigation into the effect of backpressure on the mechanical behavior of methane-hydrate-bearing sediments via DEM analyses. Comput Geotech 2015;69:551–63.
[37] Jiang M, Shen Z, Wang J. A novel three-dimensional contact model for granulates incorporating rolling and twisting resistances. Comput Geotech 2015;65:147–63.
[38] Jing L, Kwok CY, Leung AYF, Sobral Y. Extended CFD-DEM for free-surface flow with multi-size granules. Int J Numer Anal Meth Geomech 2015;40(1):62–79.
[39] Johnson KL. The correlation of indentation experiments. J Mech Phys Solids 1970;18(2):115–26.
[40] Johnson KL. Contact mechanics. Cambridge University Press; 1985.
[41] Kang DH, Choo J, Yun TS. Evolution of pore characteristics in the 3D numerical direct shear test. Comput Geotech 2013;49:53–61.
[42] Kendall K. The stiffness of surfaces in static and sliding contact (Doctoral dissertation). University of Cambridge; 1969.
[43] Lim WL, McDowell GR. Discrete element modelling of railway ballast. Granular Matter 2005;7(1):19–29.
[44] Marks B, Einav I. A cellular automaton for segregation during granular avalanches. Granular Matter 2011;13(3):211–4.
[45] Marks B, Einav I. A heterarchical multiscale model for granular materials with evolving grainsize distribution. Granular Matter 2017;19(3):61. https://doi.org/10.1007/s10035-017-0741-6.
[46] Mindlin RD, Deresiewicz H. Elastic spheres in contact under varying oblique forces. J Appl Phys 1953:327–43.
[47] Nardelli V. An experimental investigation of the micromechanical contact behavior of soils. Architechture and Civil Engineering Department. City University of Hong Kong; 2017.
[48] Nardelli V, Coop MR, Andrade JE, Paccagnella F. An experimental investigation of the micromechanics of Eglin sand. Powder Technol 2017;312:166–74.
[49] Ni J, Zhu Z. Experimental study of tangential micro deflection of interface of machined surfaces. J Manuf Sci Eng 2001;123(2):365–7.
[50] O'Sullivan C. Particle-based discrete element modeling: geomechanics perspective. Int J Geomech 2011;11(6):449–64.
[51] Olsson E, Larsson PL. On the tangential contact behavior at elastic–plastic spherical contact problems. Wear 2014;319(1–2):110–7.
[52] Peyret N, Dion JL, Chevallier G, Argoul P. Micro-slip induced damping in planar contact under constant and uniform normal stress. Int J Appl Mech 2010;2(02):281–304.
[53] Proprentner D. Friction, wear and tangential stiffness of metal surfaces under fretting conditions. Department of Mechanical Engineering. Imperial College London; 2012.
[54] Sandeep CS, Todisco MC, Nardelli V, Senetakis K, Coop MR, Lourenco SDN. A micro-mechanical experimental study of highly/completely decomposed tuff granules. Acta Geotech 2018. https://doi.org/10.1007/s11440-018-0656-3.
[55] Sandeep CS, He H, Senetakis K. An experimental micromechanical study of sand grain contacts behavior from different geological environments. Eng Geol 2018;264:176–86.
[56] Sandeep CS, Senetakis K. Effect of Young's modulus and surface roughness on the inter-particle friction of granular materials. Materials 2018;11:217.
[57] Sandeep CS, Senetakis K. Grain-scale mechanics of quartz sand under normal and tangential loading. Tribol Int 2018;117:261–71.
[58] Sandeep CS, Senetakis K. Micromechanical experiments using a new inter-granule loading apparatus for gravel-to-ballast sized materials. Friction 2018. https://doi.org/10.1007/s40544-018-0243-5. (In press).
[59] Sazzad MM, Suzuki K. Effect of inter-particle friction on the cyclic behavior of granular materials using 2D DEM. J Geotech Geoenviron Eng 2011;137(5):545–9.
[60] Senetakis K, Coop M, Todisco MC. The inter-particle coefficient of friction at the contacts of Leighton Buzzard sand quartz minerals. Soils Found 2013;53(5):746–55.
[61] Senetakis K, Coop MR. The development of a new micro-mechanical inter-particle loading apparatus. Geotech Test J 2014;37(6):1028–39.
[62] Senetakis K, Sandeep CS, Todisco MC. Dynamic inter-particle friction of crushed limestone surfaces. Tribol Int 2017;111:1–8.
[63] Shen WG, Zhao T, Zhao JD, Dai F, Zhou GD. Quantifying the impact of dry debris flow against a rigid barrier by DEM analyses. Eng Geol 2018;241:86–96. https://doi.org/10.1016/j.enggeo.2018.05.011.
[64] Soga K, O'Sullivan C. Modeling of geomaterials behavior. Soils Found 2010;50(6):861–75.
[65] Tang CL, Hu JC, Lin ML, Angelier J, Lu CY, Chan YC, et al. The Tsaoling landslide triggered by the Chi-Chi earthquake, Taiwan: insights from a discrete element simulation. Eng Geol 2009;106(1–2):1–19.
[66] Thornton C, Barnes DJ. Computer simulated deformation of compact granular assemblies. Acta Mech 1986;64(1–2):45–61.
[67] Ting JM, Corkum BT, Kauffman CR, Greco C. Discrete numerical model for soil mechanics. J Geotech Eng 1989;115(3):379–98.
[68] Todisco MC, Wang W, Coop MR, Senetakis K. Multiple contact compression tests on sand particles. Soils Found 2017;57(1):126–40.
[69] Utili S, Nova R. DEM analysis of bonded granular geomaterials. Int J. Numer Anal Meth Geomech 2008;32(17):1997–2031.
[70] Vu-Quoc L, Zhang X, Lesburg L. Normal and tangential force–displacement relations for frictional elasto-plastic contact of spheres. Int J Solids Struct 2001;38(36–37):6455–89.
[71] Yan Z, Wilkinson SK, Stitt EH, Marigo M. Discrete element modelling (DEM) input parameters: understanding their impact on model predictions using statistical analysis. Comput Particle Mech 2015;2(3):283–99.
[72] Yasar E, Erdogan Y. Correlating sound velocity with the density, compressive strength and Young's modulus of carbonate rocks. Int J Rock Mech Min Sci 2004;41(5):871–5.
[73] Yin ZY, Zhao JD, Hicher PY. A micromechanics-based model for sand-silt mixtures. Int J Solids Struct 2014;51(6):1350–63.
[74] Zhang X, Vu-Quoc L. An accurate elasto-plastic frictional tangential force–displacement model for granular-flow simulations: displacement-driven formulation. J Comput Phys 2007;225(1):730–52.